RSC Advances

ROYAL SOCIETY OF CHEMISTRY

www.rsc.org/advances

ASSESSMENT OF EFFECTS OF MULTI DRUG RESISTANCE ON DIELECTRIC PROPERTIES OF K562 LEUKEMIC CELLS USING ELECTROROTATION

Garsha Bahrieh[a,c], Murat Erdem[b], Ebru Özgür[c], Ufuk Gündüz[b], Haluk Külah[a,c,1]

[a]Department of Electrical and Electronics Engineering, METU, Ankara, Turkey
[b]Department of Biology, METU, Ankara, Turkey
[c]METU-MEMS Research and Applications Center, Ankara, Turkey

Abstract

In this study, dielectric characterizations of multidrug resistant (MDR) K562 human leukemia cells were carried out using MEMS based electrorotation (ER) device with 3D electrodes. P-glycoprotein (P-gp) dependent MDR causes variation in cell dielectric properties (cell interior conductivity (σ_i), membrane capacitance (C_m) and total effective membrane conductance (G_m^*)) due to overexpression of P-gp, which modulates the activity of membrane-bound Cl^- channels. Different cell populations resistant to varying levels of doxorubicin (DOX, 0.1-0.5 µM) and imatinib (IMA, 0.2-0.5 µM) were studied to reveal the relationship between cell dielectric properties and degree of drug resistance. ER characterization results proved considerable changes in cells membrane and interior dielectric properties as the resistance level to chemotherapeutic drugs change. The membrane dielectric properties of the cells increase significantly at low (0.1 – 0.2 µM) drug resistance levels (K562/IMA-0.2: C_m=15.63±3.02 mF m^{-2} and G_m^*=2953±82 S m^{-2}, and K562/DOX-0.1: C_m=12.29±2.15 mF m^{-2} and G_m^*=1810±14 S m^{-2}), compared to the sensitive ones (C_m=8.93±1.43 mF m^{-2} and G_m^*=336±73 S m^{-2}). However, they follow a decreasing trend as the drug resistance level increases (0.3 – 0.5 µM). The membrane capacitance and effective conductance for IMA resistant K562 cells falls to 8.10±1.69 mF m^{-2} and 113±18 S m^{-2} in 0.5 µM resistant cells, respectively. Similarly, the membrane capacitance and effective conductance of DOX resistant cells falls to 8.70±1.71 mF m^{-2} and 1377±22 S m^{-2} in 0.5 µM resistant cells, respectively. However, no direct relationship could be observed between increased drug resistance and cell interior conductivity, which showed an oscillating behavior. Results prove that degree of drug resistance significantly affects the dielectric properties of K562 cells, although they possess a similar size and morphology. Variations in cells dielectric properties results in differentiations in DEP crossover frequencies, which could be utilized in the detection and separation of MDR using dielectrophoretic based devices.

[1] METU, Department of Electrical and Electronics Engineering, Ankara, Turkey.

Phone: +90 312 210 2345, Fax: +90 312 210 2304, e-mail: kulah@metu.edu.tr

Keywords: K562 cells, multidrug resistance, electrorotation, cell dielectric properties, doxorubicin, imatinib.

1. Introduction

MDR is defined as the resistance of cancer cells to chemotherapeutic drugs with distinct chemical structures[1], and represents a significant challenge in effective cancer treatment through chemotherapy. There are various mechanisms employed by cancer cells to develop resistance against drugs[2]. Understanding these mechanisms and effects of MDR in cancer cells, and developing methods to detect it in the early stages is a growing interest in present-day cancer researches. Study of the dielectric properties of MDR cancer cells not only enhances our understanding of MDR development, but also can provide means to detect MDR in the early stages and help monitor response to therapy. The most common mechanism in MDR is the overexpression of membrane-associated drug efflux pumps, mainly the multidrug resistance associated protein (MRP) and P-glycoprotein (P-gp), through which cells effectively decreases the intracellular concentration of drugs below their cytotoxic levels. The chemotherapeutic drugs, Doxorubicin (DOX) and Imatinib (IMA), used in the treatment of chronic myeloid leukemia (CML) and in a variety of other malignancies, are known to cause MDR by overexpression of P-gp[3–5]. The overexpression of P-gp is associated with the variation in cytoplasmic ion concentration and membrane electrical properties, most probably through its modulatory effect on volume-activated Cl^- channels[6,7]. It was reported that 0.1 μM DOX resistant K562 leukemic cells, overexpressing P-gp, have an increased cytoplasmic conductivity compared to the sensitive cells and that variation is not affected by the presence of MDR reversal agent[1]. The resistant cells were reported to have higher cytoplasmic Cl^- levels as validated by using ion channel blockers[8]. The variation in cytoplasmic conductivity and membrane dielectric properties due to overexpression of P-gp can be utilized as a distinctive feature to separate sensitive cells from the resistant ones through dielectrophoresis (DEP) based approaches[9].

Cell dielectric characterization can be realized through a variety of methods, including Electrorotation (ER), DEP[10,11], microelectrical impedance spectroscopy (μ-EIS)[12–14], or impedance flow cytometry (IFC)[15–19]. ER is the only practical method for extracting the cells membrane and interior dielectric properties accurately[20]. ER is a phenomenon associated with rotation of dielectric particles under uniformly rotating electric field[21–23]. The frequency dependent rotation speeds of particles in media with different conductivities are used to estimate their surface and interior dielectric properties, including membrane capacitance (C_M), total effective membrane conductance (G_m^*), and intracellular conductivity (σ_i), at the single cell level. ER have been successfully used in dielectric characterization of biological

cells, including erythrocytes[24,25], leukocytes[26–30], fibroblasts[31], variety of cancer cells[1,32,33], and bacterial cells[34].

In this study, dielectric characterization of sensitive and MDR K562 cells were determined through electrorotation (ER) method to reveal the effect of resistance level on cells intracellular and membrane dielectric properties. For this purpose, a microfabricated ER device with 3D polynomial electrodes was utilized. Dielectric properties of MDR K562 cells with different resistance levels to chemotherapeutic drugs, DOX (0.1, 0.3 and 0.5 μM) and IMA (0.2, 0.3 and 0.5 μM), together with the sensitive parental K562 cells were investigated. Dielectric properties of membrane (capacitance and total effective conductance) and cytoplasm (conductivity) were determined by measuring the frequency dependent rotation rate of cells in media with different conductivities.

Results have shown that there are significant variations in the cytoplasmic conductivity of the sensitive and resistant cells with low drug resistance levels (0.1 and 0.2 μM), which is in correlation with the results reported previously using 0.1 μM DOX resistant K562 cells via DEP collection spectroscopy technique[1,35]. However, we observed that there is no linear correlation between the degree of drug resistance and cytoplasmic conductivity, which showed an oscillating behavior at different degrees of drug resistance, for both types of the resistant cell lines. In cells with low resistance levels, there was an increase in membrane capacitance and membrane effective conductance, which showed a decay as the resistance degree increased to 0.5 μM, and finally reached to the level of sensitive ones. These results imply the presence of different levels of regulation mechanisms depending on the degree of resistance which can be revealed with further molecular characterizations, including P-gp and Cl^- channel activities and expression levels.

2. Theory and Mathematical Methodology

ER is a phenomenon associated with rotation of polarizable particles under uniformly rotating electric field. The rotational torque is generated by the interaction of rotating electric field with induced dipole moment on the particles. Rotating electric field is generated by application of four sinusoidal signals in phase quadrature to the quadruple electrodes (Fig. S1 in the ESI). For a spherical particle of radius R, under a uniformly rotating electric field of strength *E*, the frequency dependent torque (*T*) is given as[22]:

$$T = -4\pi\varepsilon_{med}R^3\mathrm{Im}(F_{CM})E^2 \quad (1)$$

where, ε_{med} is the permittivity of the suspension medium and F_{CM} is the complex Clausius-Mossoti factor, represented by:

$$F_{CM} = Re(F_{CM}) + jIm(F_{CM}) = \frac{\varepsilon_p^* - \varepsilon_{med}^*}{\varepsilon_p^* + 2\varepsilon_{med}^*} \quad (2)$$

where, $j = \sqrt{-1}$, ε_p^* and ε_{med}^* represent the complex permittivity of the particle and the medium, respectively and are given by:

$$\varepsilon_n^* = \varepsilon_n - j\frac{\sigma_n}{\omega} \quad (3)$$

where, the subscript *n* refer to the particle (p) or the medium (med), σ is the conductivity, and ω is the angular frequency of the applied electric signal. When Im(F_{CM}) > 0, the induced dipole moment on the particle lags behind the applied external electric field by less than half a period and an anti-field rotation occurs. On the other hand, when Im(F_{CM}) < 0, the induced dipole moment lags behind the external applied electric field by greater than half a period and co-field rotation occurs[23,30].

For single-shell model of biological cells with radius R and membrane thickness of δ, the ε_p^* changes to complex equivalent of cell permittivity ($\widetilde{\varepsilon_2^*}$), and is given by[23]:

$$\widetilde{\varepsilon_2^*} = \widetilde{\varepsilon_2} + j\widetilde{\sigma_2} = \varepsilon_m^*\left[\frac{(R/(R-\delta))^3 + 2(\varepsilon_i^* - \varepsilon_m^*)/(\varepsilon_i^* + 2\varepsilon_m^*)}{(R/(R-\delta))^3 - (\varepsilon_i^* - \varepsilon_m^*)/(\varepsilon_i^* + 2\varepsilon_m^*)}\right] \quad (4)$$

where, ε_m^* is the complex cell membrane permittivity and ε_i^* is the complex cell interior permittivity. However, the single-shell model is an approximation of complex cell structure and includes all cells interior compositions like cytoplasm and nucleus as a single layer.

The peak rotation frequency for a specific cell can be obtained by setting $\frac{dIm(F_{CM})}{d\omega} = 0$, which results in Equation (5) for peak rotation frequency (f_{pk}):

$$\omega_{pk} = 2\pi f_{pk} = \frac{\tilde{\sigma}_2 + 2\sigma_{med}}{\tilde{\varepsilon}_2 + 2\varepsilon_{med}} \quad (5)$$

Under low frequency (DC-limit) approximations, Equation 5 can be simplified as[22,36,37]:

$$\mathrm{Rf_{PK}} = \frac{\sigma_{med}}{\pi \mathrm{C_m}} + \frac{\mathrm{G_m^* R}}{2\pi \mathrm{C_m}} \quad (6)$$

where, C_m is the transmembrane capacitance and G_m^* is the total effective membrane conductance. Equation 6 provides a linear formulation as a function of peak rotation frequency, cell radius, and medium conductivity (σ_{med}). The plot of $\mathrm{Rf_{PK}}$ against σ_{med} is expected to be linear, in the form of a straight line expression, $y = \boldsymbol{m}x + \boldsymbol{c}$, where m and c are:

$$\mathrm{m} = \frac{1}{\pi \mathrm{C_m}} \quad (7a)$$

and

$$c = \frac{R}{2\pi C_m}\left(\frac{2K_{ms}}{r^2} + G_m\right) \quad (7b)$$

For most of mammalian cells, R is in the range of a few micrometers, and δ is a few tens of nanometers. In addition, by using the DC limit approximations provided by Lei et al. for peak rotation frequencies below 1 MHz and medium conductivities below 100 mS m^{-1}, Equation 4 can be simplified as[37]:

$$\frac{\tilde{\varepsilon}_2}{\varepsilon_0} = \frac{\frac{{\sigma_i}^2}{\omega^2\varepsilon_0^2}\left(\frac{\varepsilon_m}{\varepsilon_0}\right)\left(\frac{\delta}{R}\right)}{\left(\frac{\varepsilon_m}{\varepsilon_0}\right)^2 + \frac{{\sigma_i}^2}{\omega^2\varepsilon_0^2}\left(\frac{\delta}{R}\right)^2} \quad (8a)$$

and

$$\tilde{\sigma}_2 = \frac{\frac{\sigma_m {\sigma_i}^2}{\omega^2\varepsilon_0^2}\left(\frac{\delta}{R}\right)}{\left(\frac{\varepsilon_m}{\varepsilon_0}\right)^2 + \frac{{\sigma_i}^2}{\omega^2\varepsilon_0^2}\left(\frac{\delta}{R}\right)^2} \quad (8b)$$

In above equations, by limiting the peak rotation frequency to 1 MHz and medium conductivity to 100 mS/m, terms with three orders less are omitted. By substituting Equations 8a and 8b in Equation 5, below equation is obtained:

$$\sigma_i^2\left[\frac{C_m\delta^2}{\omega_{pk}\varepsilon_0^2 R} + \frac{2\varepsilon_1}{\omega_{pk}\varepsilon_0^2}\left(\frac{\delta}{R}\right)^2 - \frac{G_m\delta^2}{{\omega_{pk}}^2\varepsilon_0^2 R} - \frac{2\sigma_{med}}{{\omega_{pk}}^2\varepsilon_0^2}\left(\frac{\delta}{R}\right)^2\right] - \sigma_i\left[\left(\frac{C_m\delta}{\varepsilon_0}\right)^2\right] = \frac{2\sigma_1 {C_m}^2\delta^2}{\varepsilon_0^2} - 2\varepsilon_1\omega_{pk}\frac{{C_m}^2\delta^2}{\varepsilon_0^2} \quad (9)$$

C_m and G_m are extracted using slope and intercept of the plot relating the peak rotational frequency and cell radius with medium conductivity. ω_{pk} and σ_{med} are extracted from electrorotation experiments. Therefore, the cell interior conductivity (σ_i) can be calculated by solving the Equation 9 for σ_i.

3. Design and fabrication

Optimization analysis of various electrode structures, including pyramidal, ellipse, pin, and polynomial by Hughes et al. has shown that the polynomial structures have the most practical compromise between the generated maximum rotational torque and maximum area with uniform torque distribution[38–40]. In this study, 3D microfabricated polynomial electrodes were utilized to induce the rotational torque on the cells by applying four sinusoidal signals in phase quadrature. 3D electrodes extruded 30 µm in z-direction, encompass the whole cell structure and minimize the fringing electric field effect on the rotating cells. In addition, it provides a highly uniform electric potential distribution along the z-direction; therefore, minimizes the z-component of the electric field. By decreasing the z-component of the electric field, out of plane movements of the cells in the z-direction is

minimized. Therefore, it minimizes the variation of rotational torque and increases the uniformity within the measurement area and hence, improves the accuracy of ER measurements. Moreover, due to increased electrode surface and volume in 3D electrodes, the current density decreases, which reduce the local thermal heating effect (joule heating) on the electrodes, thereby, decreasing the variance in medium conductivity caused by changes in medium temperature[41].

Electrode structures and the gap between the electrodes (500 μm) were optimized using FEM simulations. Fig. 1 shows 3D FEM (COMSOL Multiphysics®) simulation of the effective electric field distribution and effective rotating electric field direction, in different time instants. Uniform distribution of the electric field in 3D polynomial electrodes results in reduction of the magnitude of the effective DEP force on the cells and reduces the vertical (out of focal) and horizontal (lateral) movements of the cells.

The optimized devices were fabricated using microfabrication techniques. Cross-section of the fabrication process is shown in Fig. 2a. Ti/Au sputtering was carried out on Si substrate and shaped using lithography, to form a seed layer for the Cu electroplating. 3D Cu electrodes (30 μm height) were electroplated on the patterned seed layer. A thin gold layer (250 nm) was deposited by electroless Au deposition, to prevent the interaction of the Cu electrodes with the phosphate buffered saline (PBS) containing sample medium, reducing the risk of electrolysis. Finally, a PDMS reservoir was mounted to keep the cells on the measurement area. The fabricated prototype and the SEM photograph of the 3D electrodes are shown with in Fig. 2b.

4. Experimental

4.1. Cell preparation

The Philadelphia chromosome positive K562 cell lines were obtained from the Germen Collection of Microorganisms and Cell Cultures, Germany, and cultured in RPMI 1640 medium (Invitrogen) with fetal bovine serum and penicillin-streptomycin. Imatinib (Novartis) or doxorubicin (Adriamycin, SABA) was added to culture media with gradual increments in dosage until the cells become resistant to desired level of drug concentrations (DOX: 100, 300, 500 nM; IMA: 200, 300, 500 nM)[42]. The human chronic myeloid leukemia cells (K562) and its drug resistant counterparts with different levels of resistance to imatinib (K562/IMA) and doxorubicin (K562/DOX) drugs were grown in RPMI-1640 medium, at 37°C, under 5% CO_2. Before analyzing each population, cells were washed twice by centrifuging at 1000 RPM for 5 minutes at room temperature. Finally, the pellets were re-suspended in isotonic medium, consisting of 8.5% (w/v) sucrose plus 0.3% (w/v) dextrose. Cell concentration was adjusted to $5x10^5$ cells/ml. Phosphate buffered saline

(PBS, Santa Cruz Biotechnology, 10X) was used to adjust the medium conductivities (1-8 mS m^{-1}).

4.2. Experimental Setup for Electrorotation

Before energizing the electrodes (Agilent-81150A), 3 µL of the cell suspension (in room temperature) were loaded into the PDMS reservoir of the ER device. Sinusoidal voltages in the range of 10 - 12.5 V_{PP}, in frequencies between 1 kHz and 100 kHz (with 5 kHz intervals), were applied to electrodes, by using 50Ω coaxial cables with BNC connections. The voltage was optimized by FEM studies of the effective electric field (EEF) and DEP force magnitude and tested experimentally to adjust the rotation rate at a manually measurable range (180-240 RPM). The cells in the PDMS reservoir were replaced with fresh cells several times during each experiment, in order to reduce the possibility of change in cells dielectric properties due to the application of external electric field. Rotation of cells was recorded using a video microscope (Karl Suss, PM5). The experimental setup is shown in Fig. 3. The boundary of the measurement area was optimized using FEM analysis to minimize the variation of the rotational torque. Fig. 4a shows the simulation of the effective electric field distribution over the device surface. The changes of the EEF were studied along four lines separated by 45° passing through the device center. A circular area with a radial length of approximately 50 µm from the electrodes center was chosen for the measurements. According to Fig. 4b, in this area, the maximum variation of the generated rotational torque is less than 15% compared to the central torque.

One of the challenging issues in ER tests is the immobilization of cells in their position while a rotating electric field is applied. Therefore, the amplitude of the rotational torque remains constant, which increases the reliability of the collected data. Different methodologies are suggested and developed for immobilizing cells, including use of laser tweezers[29,43–47] and DEP-cages[44,47,48]. In this study, cells were kept in the center of the electrode tips by utilizing the repulsive negative DEP (nDEP) force. In the low ionic strength media (around 10^{-3} S m^{-1}), K562 cells observe nDEP force, at the applied frequency range. Under nDEP force, cells experience a repulsive force from the electrode tips and are trapped in the center of the electrodes, where the electric field gradient intensity is lower (nDEP region). Detailed FEM simulations of the DEP forces in the inter-electrode region of the devices are provided in ESI (Fig. S2). Moreover, the use of low ionic medium conductivities reduces the joule heating and electrolysis effects[24,26].

At each frequency step, rotation rates were measured for 12 different cells placed within the defined circular boundaries. To minimize the influence of the cells from the dipole moment of nearby rotating cells, measurements were limited to the cells separated by at least three

cell diameters from nearby cells[30]. Each test was repeated twice, ascending from 1 kHz to 100 kHz and descending to 1 kHz with 5 kHz intervals. Peak rotation frequency in each medium with specific conductivity was calculated based on the average of the collected rotation rates. Instead of selecting a specific peak frequency, a peak frequency with a deviation range was chosen. This averaging was used in the calculation of cells' average dielectric properties and the standard deviations.

5. Results and Discussions

The aim of this study is to investigate the variation in dielectric properties of sensitive and MDR K562 cells with different levels of resistance to chemotherapeutic drugs, DOX and IMA, through ER technique and to evaluate the feasibility of detection and separation of MDR in human leukemia using DEP approach. The peak rotation frequencies (f_{pk}) of cells at different medium conductivities were measured to estimate the cells' dielectric properties, including the total effective membrane conductance, membrane capacitance, and intracellular conductivity. The ER spectrum of the cells includes two peak rotation frequencies, in low and high frequency ranges. In this study, we have used the first peak (low frequency, <100 kHz) rotation frequency to extract the cell membrane and interior dielectric properties. Low ionic strength media, with conductivities lower than 10 mS m^{-1}, was used to satisfy the low frequency (DC) approximation for equivalent permittivity and conductivity expressions of the single-shell cell model.

The ER spectrum of K562/IMA-0.2, 0.3, and 0.5 µM resistant cells in different medium conductivities, in the frequency range of 1 kHz – 0.1 MHz are shown in Fig. 5a-c. Subsequent to measurement of peak rotation frequencies of each cell population in medium conductivities ranging from 1 to 8 mS/m, the expression of the straight line was fitted to data points of the peak rotation frequency and cell radius versus medium conductivity (Fig. 5d). The same approach was followed for K562/DOX- 0.1, 0.3, and 0.5 µM cells (Fig. 6) and K562 drug sensitive cells (Fig. 7). The ER spectrum of the K562/DOX and sensitive cells are provided in the ESI section (Fig. S3 and Fig. S4). Standard deviations were calculated for each data point based on variations in cell sizes and deviations in peak rotation frequencies. For characterization of each cell type, rotation of approximately 1000 cells were studied in the frequency range of 1 – 100 kHz inside four media with varying conductivities (1-8 mS $m^{=1}$). Automated MATLAB® algorithm was used for calculating the dielectric properties of the cells using straight line fitting. The slope and intercept point of the fitted straight line was used for calculation of cell membrane capacitance and effective membrane conductance, respectively, using Equation 6. Cells interior conductivity is calculated using Equations 8a, 8b, and 9. The extracted cell dielectric properties with standard deviations are given in Table 1. The membrane capacitance for K562/IMA-0.2 (15.63±3.02 mF m^{-2}) and K562/DOX-0.1

(12.29±2.15 mF m^{-2}) cells are considerably higher than the membrane capacitance for drug sensitive cells (8.93±1.43 mF m^{-2}). However, as the level of drug resistance increases, the membrane capacitance decreases. For the 0.5 μM drug resistant cells, the membrane capacitance decreases to the levels of sensitive cells. The same trend was followed for the total effective membrane conductance, the magnitude of which gradually decreased as the level of resistance to IMA and DOX increased. However, no direct relationship could be observed with the degree of drug resistance and cell interior conductivity, which exhibited an oscillating behavior.

Calculation of cells interior permittivity needs the full expression for the cells effective permittivity and conductivity, and could not be extracted with implemented equations in this study. Labeed et al. has reported a range of 40-80 for cytoplasmic permittivity of K562 and K562AR (DOX), hence, an average value of 60 can be considered for the cell interior permittivity[1].

DEP spectrum of the characterized cells is simulated using MATLAB (Fig. 8), based on the presented data in Table 1. In this simulation, the conductivity and relative permittivity of the suspension medium is assumed as 1mS m^{-1} and 78, respectively. The average value of 60 is considered for relative interior permittivity of the cells. At low frequencies (< 1 MHz), DEP spectrum is dominated by the membrane capacitance and conductance. However, with increasing frequency, the capacitance of the membrane shorts out the membrane conductance and cells interior properties become dominant (electric field senses the dielectric properties of the cell interior). Due to differences in cells membrane capacitance and effective conductance and interior conductivity, each cell population exhibit particular DEP response in low and mid-frequency ranges. With increasing frequency (>100MHz), cell interior permittivity specifies the DEP spectrum. Assuming the value of 60 for cell interior permittivity had led to similar DEP response in frequencies above 100 MHz, under given medium conditions.

6. Conclusion

In this study, dielectric characterizations of K562 human leukemia cells and its MDR counterparts were carried out using ER technique with 3D electrodes. 3D electrode structures have variety of advantages over generally used planar electrodes including: (i) It eliminates the fringing electric field effect on the cells rotation by encompassing the whole cell body, (ii) it generates a uniform electric field distribution along the z-direction, (iii) out of plane movements of the cells are prevented due to minimized variations of z-component of the electric field, and, (iv) due to minimized thermal heating effect on the 3D electrode structures, the temperature-dependent changes in the medium conductivity are reduced considerably (around an order of magnitude, as investigated using FEM

analysis). All of these have contributed to increased accuracy in ER measurements. Use of low ionic strength media (1-8 mS m^{-1}) and low frequency (1-100 kHz) resulted in the nDEP response of the cells over the wide frequency range, which minimized the lateral movement of cells during measurements. Assumptions in simplifying the expression of complex equivalent of cell permittivity limited the maximum peak rotation frequency and medium conductivity to 1 MHz and 100 mS m^{-1}, respectively, which were satisfied in this study[37]. It is important to note that, the calculated peak rotation frequencies are in the range of 10 – 65 kHz, therefore the electrode polarization effect can be neglected. The polarization effect is significant in the frequencies below 1 kHz[49]. In addition, in the ER measurements presented in this study, the rotations of the cells were studied at least 200 μm far from the electrodes tips (a circular area with a radius of 50 μm at the center of the inter-electrode region). Therefore, the influence of the generated double-layer capacitance can be neglected.

The cytoplasmic membrane is the primary site of cell's response to different environmental stresses and it initiates secondary responses through a signal transduction system. This leads to triggering of a complex set of regulatory mechanisms to cope with the stress and to survive, eventually. One of the mechanisms of developing resistance to chemotherapeutic agents is to overexpress drug efflux proteins embedded in the cytoplasmic membrane, leading to reduced exposure of cytoplasmic structures to the toxic effect of the drugs. This variation in cytoplasmic membrane structure and function leads to variation in dielectric properties of the membrane and the cytoplasm, which may be utilized as a tool to detect MDR in cancer cells. In this study, ER characterization results prove variations in membrane and cytoplasmic dielectric properties as cells develop resistance to chemotherapeutic drugs. Development of resistance to chemotherapeutic drugs in sensitive K562 cells is associated with an increase in the expression of membrane-bound drug efflux pumps (P-gp), which is known to modulate the activity of outward rectifying, volume-activated Cl^- channels[6,7]. This modulation seems to result in an increase in total effective membrane conductance (total effective membrane conductance includes the conductance across the membrane associated with ion flux through the membrane channels and pores) at low drug resistance levels (0.1-0.2 μM). With an increase in surface conductance of the membrane, the capacitance and permittivity of the membrane also increase. However, our findings have shown that further increase in drug resistance level in MDR cells results in a gradual decrease in above dielectric properties, and finally reaching to the levels of sensitive cells at 0.5 μM resistance level. This reversal in dielectric properties of the membrane may imply a different mechanism of rising resistance when cells are exposed to higher drug concentrations. The expression levels and the modulatory role of P-gp should be investigated in detail to reveal the mechanism of resistance at high drug concentrations.

Our results also indicate that the response of K562 cells to IMA and DOX in terms of effective membrane conductance shows variations. K562/IMA cells exhibited a significant increase (around

an order of magnitude) in membrane effective conductance at low drug resistance level (0.2 μM), followed by a rapid reversal to the levels of sensitive cells when drug resistance level increases. K562/DOX cell, on the other hand, exhibited an increased total membrane effective conductance at low drug resistance level, and this was stored to a large extent by the increase in drug resistance. Membrane conductance is associated with the presence and the activity of membrane proteins and ion channels, which actively engage in the cell homeostatic control. Although these chemotherapeutic drugs are known to cause MDR with a similar mechanism (P-gp overexpression), induced changes in membrane protein expression and activity levels and subsequent changes in ion conductance may show variation, leading to differences in membrane conductance between IMA and DOX resistant cells. These findings should be supported with further molecular characterization, including P-gp and ion channel activity and expression levels, of K562 cells with varying levels of drug resistance.

Although there is a definite trend in membrane dielectric properties with varying levels of resistance, the cytoplasmic conductivity values did not show such a trend, as shown in Table 1. Although there is a change in cytoplasmic conductivity, no correlation could be driven in relation to the drug resistance level, for both IMA and DOX resistant cells.

The results of this study reveal significant variation in cell dielectric properties of sensitive and resistant cancer cells, which can be utilized as an effective tool to detect MDR through DEP based methods. With the obtained dielectric properties, MATLAB simulations of the DEP spectrum have been carried out, showing that MDR cells can be differentiated from the sensitive ones through DEP. Such a system can be used effectively in the future to detect MDR before and during chemotherapy.

Acknowledgement

The authors acknowledge the Scientific and Technological Research Council of Turkey (TUBITAK) for the financial support through project 111E194. The authors would like to thank Aziz Koyuncuoğlu and Dr. Özge Zorlu for their assistance in the fabrication of ER chips.

References

1. F. H. Labeed, H. M. Coley, H. Thomas, and M. P. Hughes, *Biophys. J.*, 2003, **85**, 2028–2034.

2. R. Krishna and L. D. Mayer, *Eur. J. Pharm. Sci.*, 2000, **11**, 265–283.

3. K. S. Yang, Chun Zheng; Luan, Feng Jun; Xiong, Dong Sheng; Liu, Bin Ren; Xu, Yuan Fu; Gu, *Acta Pharmacol. Sin.*, 1995, **16**, 333–337.

4. T. Illmer, M. Schaich, U. Platzbecker, J. Freiberg-Richter, U. Oelschlägel, M. von Bonin, S. Pursche, T. Bergemann, G. Ehninger, and E. Schleyer, *Leukemia*, 2004, **18**, 401–408.

5. Y. Assef, F. Rubio, G. Coló, S. del Mónaco, M. a Costas, and B. a Kotsias, *Leuk. Res.*, 2009, **33**, 710–716.

6. Y. a Assef, S. M. Cavarra, A. E. Damiano, C. Ibarra, and B. a Kotsias, *Leuk. Res.*, 2005, **29**, 1039–1047.

7. H. T. Idriss, Y. A. Hannun, E. Boulpaep, and S. Basavappa, *J. Physiol.*, 2000, **524**, 629–636.

8. L. Duncan, H. Shelmerdine, M. P. Hughes, H. M. Coley, Y. Hübner, and F. H. Labeed, *Phys. Med. Biol.*, 2008, **53**, N1–7.

9. Y. Demircan, A. Koyuncuoğlu, M. Erdem, E. Özgür, U. Gündüz, and H. Külah, in *Transducers*, Barcelona, SPAIN, 2013, vol. 1, pp. 2086–2089.

10. F. F. B. and P. R. G. Y. Huang, X. B. Wang, *Biophys. J.*, 1997, **73**, 1118–1129.

11. K. F. H. and M. P. H. H. O. Fatoyinbo, *Electrophoresis*, 2008, **28**, 3–10.

12. T. Sun and H. Morgan, *Microfluid. Nanofluidics*, 2010, **8**, 423–443.

13. L.-S. Jang and M.-H. Wang, *Biomed. Microdevices*, 2007, **9**, 737–743.

14. D. Malleo, J. T. Nevill, L. P. Lee, and H. Morgan, *Microfluid. Nanofluidics*, 2010, **9**, 191–198.

15. S. Gawad, L. Schild, and P. H. Renaud, *Lab Chip*, 2001, **1**, 76–82.

16. K. Cheung, S. Gawad, and P. Renaud, *Cytometry. A*, 2005, **65**, 124–132.

17. H. Benazzi, G. Holmes, D. Sun, T. Mowlem, M.C. Morgan, *IET Nanobiotechnology*, 2007, **1**, 94–101.

18. D. Holmes, D. Pettigrew, C. H. Reccius, J. D. Gwyer, C. van Berkel, J. Holloway, D. E. Davies, and H. Morgan, *Lab Chip*, 2009, **9**, 2881–2889.

19. K. C. Cheung, M. Di Berardino, G. Schade-Kampmann, M. Hebeisen, A. Pierzchalski, J. Bocsi, A. Mittag, and A. Tárnok, *Cytometry. A*, 2010, **77**, 648–666.

20. Y. Zheng, J. Nguyen, Y. Wei, and Y. Sun, *Lab Chip*, 2013, **13**, 2464–2483.

21. Herbert A Pohl, *Dielectrophoresis*, Cambridge University Press, Cambridge, 1978.

22. W. M. Arnold and U. Zimmermann, *J Naturwissenschaften*, 1982, **37c**, 908–915.

23. T. B. Jones, *Electromechanics of Particles*, Cambridge University Press, Cambridge, 1995.

24. J. Gimsa, T. Müller, T. Schnelle, and G. Fuhr, *Biophys. J.*, 1996, **71**, 495–506.

25. R. Georgieva, B. Neu, V. M. Shilov, E. Knippel, a Budde, R. Latza, E. Donath, H. Kiesewetter, and H. Bäumler, *Biophys. J.*, 1998, **74**, 2114–20.

26. S.-I. Han, Y.-D. Joo, and K.-H. Han, *Analyst*, 2013, **138**, 1529–1537.

27. D. M. Vykoukal, P. R. C. Gascoyne, and J. Vykoukal, *Integr. Biol. (Camb).*, 2009, **1**, 477–484.

28. U. Z. Xun Hu, W.Michael Arnold, *Biochim. Biophys. Acta - Biomembr.*, 1990, **1021**, 191–200.

29. J. Yang, Y. Huang, X. Wang, X. B. Wang, F. F. Becker, and P. R. Gascoyne, *Biophys. J.*, 1999, **76**, 3307–3314.

30. A. W. Griffith and J. M. Cooper, *Anal. Chem.*, 1998, **70**, 2607–2612.

31. V. Berardi, C. Aiello, A. Bonincontro, and G. Risuleo, *J. Membr. Biol.*, 2009, **229**, 19–25.

32. F. F. Becker, X. B. Wang, Y. Huang, R. Pethig, J. Vykoukal, and P. R. Gascoyne, *Proc. Natl. Acad. Sci. U. S. A.*, 1995, **92**, 860–864.

33. M. Cristofanilli, G. De Gasperis, L. Zhang, M.-C. Hung, A. Peter R. C. Gascoyne, and G. N. Hortobagyi, *Clin. Cancer Res.*, 2002, **8**, 615–619.

34. R. Hölzel, *Biochim. Biophys. Acta*, 1999, **1450**, 53–60.

35. F. H. Labeed, H. M. Coley, and M. P. Hughes, *Biochim. Biophys. Acta*, 2006, **1760**, 922–929.

36. R. Pethig, L. M. Jakubek, R. H. Sanger, E. Heart, E. D. Corson, and P. J. S. Smith, *IEE Proc. Nanobiotechnol.*, 2005, **152**, 189–93.

37. U. Lei, P.-H. Sun, and R. Pethig, *Biomicrofluidics*, 2011, **5**, 44109(0)–44109(16).

38. M. P. Hughes, *Phys. Med. Biol.*, 1998, **43**, 3639–3648.

39. M. Hughes, X. Wang, F. F. Becker, P. R. C. Gascoyne, and R. Pethig, *J. Phys. D*, 1994, **27**, 1564–1570.

40. M. P. Hughes, S. Archer, and H. Morgan, *J. Phys. D. Appl. Phys.*, 1999, **32**, 1548–1552.

41. P. R. C. Gascoyne, F. F. Becker, and X.-B. Wang, *Bioelectrochemistry Bioenerg.*, 1995, **36**, 115–125.

42. Y. Baran, A. Ural, and U. Gunduz, *Hematology*, 2007, **12**, 497–503.

43. C. Reichle, T. Schnelle, T. Müller, T. Leya, and G. Fuhr, *Biochim. Biophys. Acta*, 2000, **1459**, 218–229.

44. T. Schnelle, T. Müller, C. Reichle, and G. Fuhr, *Appl. Phys. B*, 2000, **70**, 267–274.

45. G. De Gasperis, X. Wang, J. Yang, F. F. Becker, and P. R. C. Gascoyne, *Meas. Sci. Technol.*, 1998, **9**, 518–529.

46. A. Rowe and M. Leake, *J. Mod. Opt.*, 2003, **50**, 1539–1554.

47. G. R. Fuhr and C. Reichle, *TrAC Trends Anal. Chem.*, 2000, **19**, 402–409.

48. C. Reichle, T. Müller, T. Schnelle, and G. Fuhr, *J. Phys. D. Appl. Phys.*, 1999, **32**, 2128–2135.

49. H. P. Schwan, *Biophysik*, 1966, **3**, 181–201.

Figure Legends

Fig. 1 COMSOL simulation of distribution of effective electric field on the device surface. The electrode tips have the maximum electric field value and it reduces gradually towards the electrodes center. 3D cones show the direction of the rotating effective electric field at each time instant.

Fig. 2 (a) Single mask fabrication flow of ER devices. (b) Photograph of the fabricated prototype, with SEM photograph of the 3-D electrodes (30 µm height).

Fig. 3 ER test setup. Micropipette was used for loading 3µl of cells suspension into the PDMS reservoir. Rotational torque was generated on the cells by energizing the polynomial electrodes with sinusoidal signals in phase quadrature. The rotations of the cells were recorded using a video microscope for further analysis.

Fig. 4 (a) Height presentation of effective electric field distribution on the device surface. (b) Changes of the effective electric field distribution along four lines passing through the electrodes center. In the bounded area of 50 µm around the device center (zero position) the variation of effective electric field is less than 15%. Variation in the effective electric field in x and y axis are similar, hence seems overlapped in the figure.

Fig. 5 Rotation rates of K562/IMA 0.2 (a), 0.3 (b), and 0.5 (c) µM cells in the frequency range of 1 kHz to 0.1 MHz, inside four different medium conductivities. (d) Straight line fitted to the data points of peak rotation frequency and cell radius versus medium conductivity. For each cell population, the membrane capacitance and effective conductance were calculated using the slope and intercept of the fitted line, respectively.

Fig. 6 Straight line fitted to the data points of peak rotation frequency of K562/DOX cells and cell radius versus medium conductivity. For each cell population, the membrane capacitance and effective conductance were calculated using the slope and intercept of the fitted line, respectively.

Fig. 7 Straight line fitted to the data points of peak rotation frequency of K562 drug sensitive cells and cell radius versus medium conductivity. The membrane capacitance and effective conductance were calculated using the slope and intercept of the fitted line.

Fig. 8 MATLAB simulation of DEP spectrum of K562 sensitive and resistant cells, in medium with conductivity of 1 mS/m and relative permittivity of 78. Cells interior relative permittivity is assumed as 60, therefore the high frequency DEP response of the cells overlaps for frequencies above 100 MHz. Low and high crossover frequencies are shown in insets.

Table 1 Extracted dielectric properties of drug sensitive and MDR K562 human leukemia cells, using ER method.

Figure 1

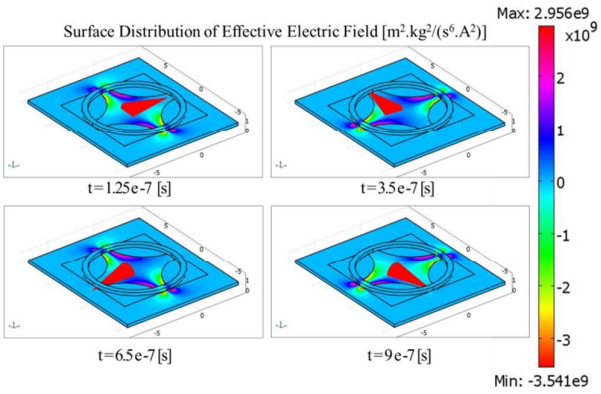

Figure 2

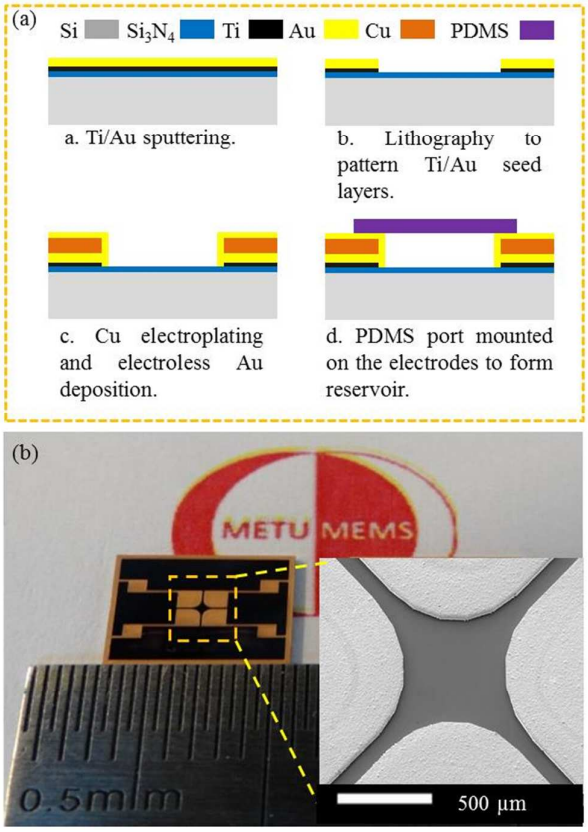

Figure 3

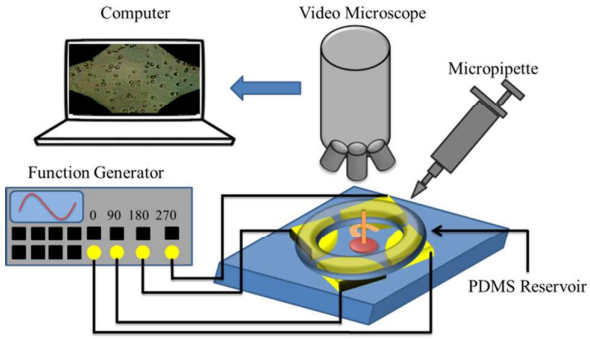

Figure 4

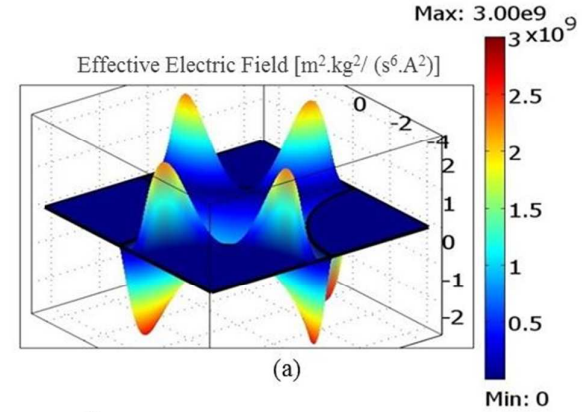

(a)

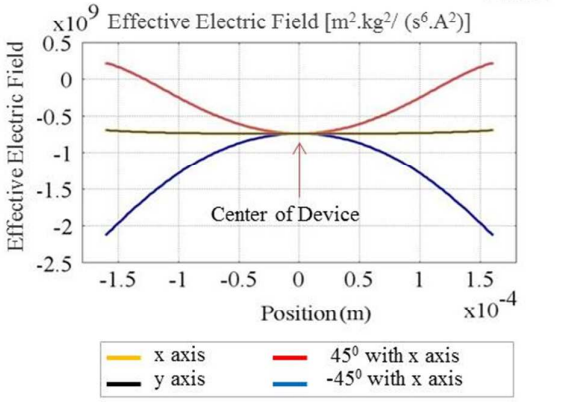

(b)

Figure 5

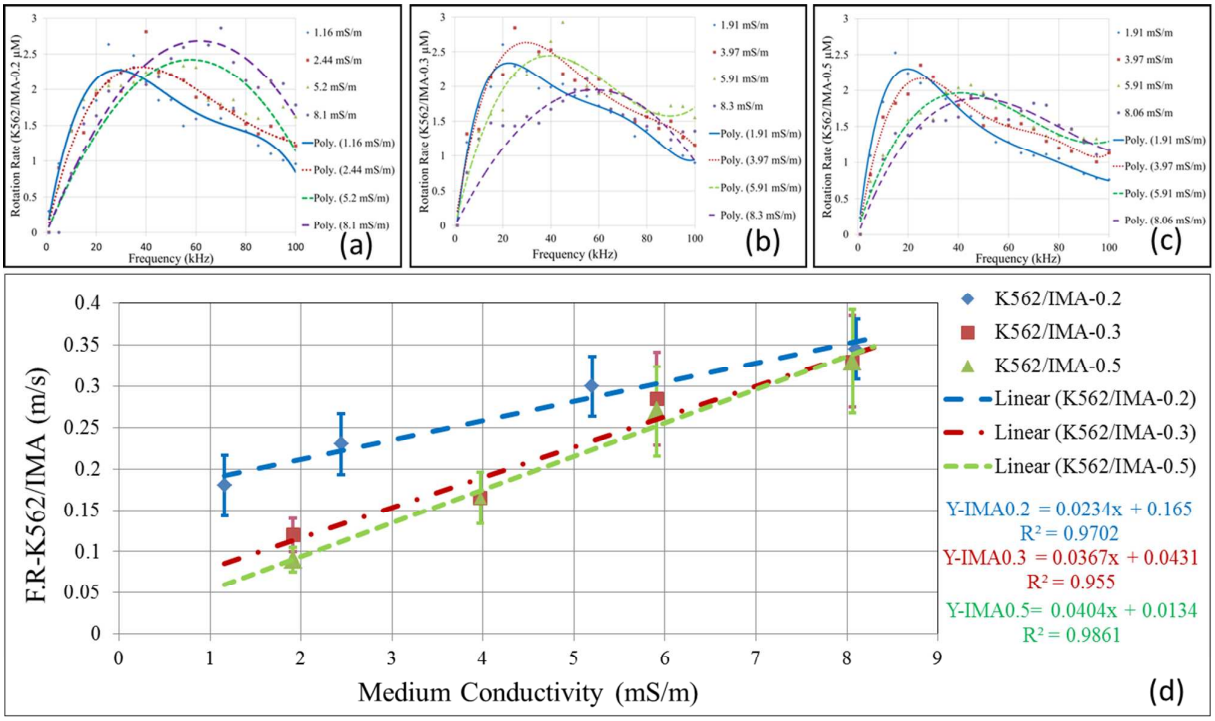

Figure 6

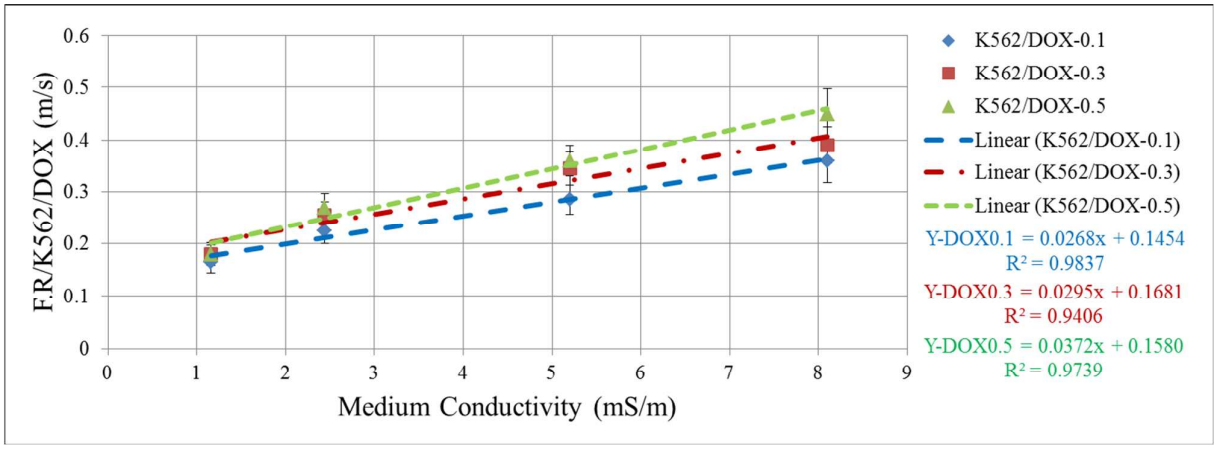

Figure 7

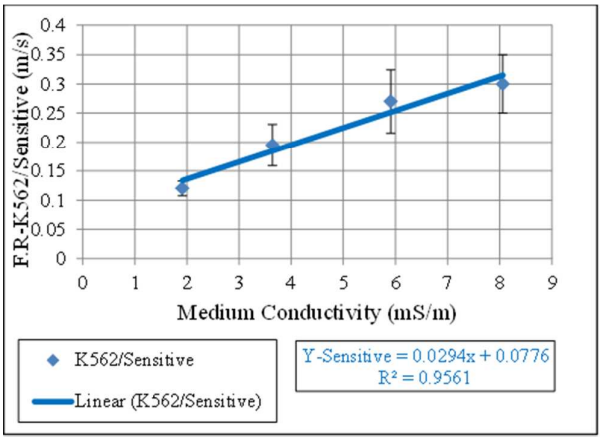

Figure 8

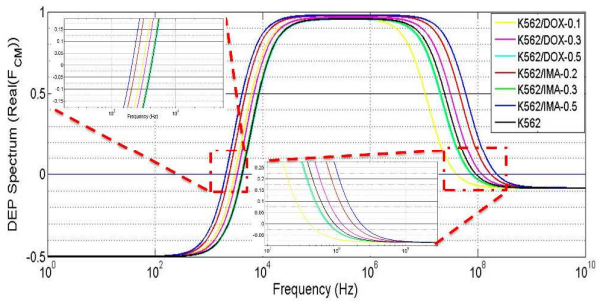

Table 1 Extracted dielectric properties of drug sensitive and MDR K562 human leukemia cells, using ER method

Cell line / Properties	Sensitive	DOX-0.1 [μM]	DOX-0.3 [μM]	DOX-0.5 [μM]	IMA-0.2 [μM]	IMA-0.3 [μM]	IMA-0.5 [μM]
Membrane capacitance [mFm^{-2}]	8.93 ± 1.43	12.29 ± 2.15	11.02 ± 1.93	8.70 ± 1.71	15.63 ± 3.02	9.19 ±1.52	8.10 ± 1.69
Membrane effective conductance [Sm^{-2}]	336 ± 73	1810 ± 14	1895 ± 59	1377 ± 22	2953 ± 82	450 ± 20	113 ± 18
Membrane relative permittivity	10.09 ± 1.61	13.89 ± 3.21	12.45 ± 2.17	9.82 ± 1.93	17.66 ± 3.41	10.38 ± 2.59	9.15 ± 2.81
Cytoplasmic conductivity [Sm^{-1}]	0.32 ± 0 .08	0.14 ± 0.01	0.41 ± 0.07	0.26 ± 0.04	0.60 ± 0.10	0.27 ± 0.10	0.78 ± 0.19
Cells radius [μm]	6 ± 1	6 ± 1	6 ± 1	6 ± 1	6 ± 1	6 ± 1	6 ± 1